Robust Control Applied to Improve the Performance of a Buck-Boost Converter

WILMAR HERNANDEZ
Universidad Politecnica de Madrid
EUIT de Telecomunicacion
Department of Circuits and Systems
Ctra. Valencia km 7, 28031 Madrid
SPAIN
whernan@ics.upm.es

Abstract: In this paper, $\mathcal{H}_\infty$ loop-shaping control is applied to improve the performance of a buck-boost dc-dc power converter based on pulse-width-modulation (PWM) techniques. Here, classical control techniques (i.e., proportional-integral-derivative (PID) control) and post-modern control techniques (i.e., $\mathcal{H}_\infty$ control), are used to design the feedback loop of a buck-boost dc-dc power converter. The results of the experiment are satisfactory and show that robust controllers do not depend strongly on the operating point, and that $\mathcal{H}_\infty$ loop-shaping control performs better than PID control.

Key–Words: buck-boost converter, state-space averaging procedure, robust stability, PID control, $\mathcal{H}_\infty$ loop-shaping control, disturbance rejection

1 Introduction

In the last two decades the classical approach to designing power converters has been transformed into the one based on the application of linear and nonlinear control techniques to improve the performance of these converters.

In [1], a nonlinear control algorithm was used to reduce the sensitivity of the control-to-output transfer function of a boost converter to the nature and magnitude of resistive loads.

Also, in [2] the most simple form of the general $\mathcal{H}_\infty$ algorithm [3–5] was applied to reduce the sensitivity of a boost converter to disturbances in the input voltage of the power converter and in its output load. What is more, Naim et al. [2] showed that dc-dc power converters whose transfer functions have right-half-plane (RHP) zeros can be controlled satisfactorily by using $\mathcal{H}_\infty$ optimal control.

Other highly regarded references on Robust Control are [6–9]

In [10], μ synthesis with DK-iteration was applied to design a robust voltage controller for a buck-boost converter with current mode control.

In [10] the μ-synthesis with DK-iteration approach yielded a much better design than the one based on PI-control.

At this point, it is should be highlighted that the nonlinear $\mathcal{H}_\infty$ control theory [11] has also been applied satisfactorily to improve the performance of a Ćuk converter, see [12].

In [12], a linear control law was used to guarantee the asymptotic stability of the closed-loop system. In addition, the controller parameters were used to adjust the performance of the closed-loop system and they were chosen taking into account heuristic considerations. Also, the control law was implemented with computer assistance.

Another application of μ synthesis with DK-iteration to improve the performance of a boost converter can be found in [13]. In that paper, the order of the controller from the DK iterations was 79 and in order to implement that controller it was necessary to reduce it to a second order controller.

In [13], the importance of including component uncertainties in the design of high-performance robust switching regulators was shown clearly.

Another application of the standard $\mathcal{H}_\infty$

control problem to improve the performance of both a boost converter and a buck-boost converter can be found in [14]. In that paper, the experimental results of the application of $\mathcal{H}_\infty$ control to designing the boost converter and the buck-boost convert were satisfactory, the tracking performance of the closed-loop systems were very good and both converters maintained their outputs closed to the desired values in the presence of disturbances.

In [15] a linear quadratic regulator (LQR) combined with a linear state estimator was used to improve the time domain performance of a $\acute{C}$uk converter.

Finally, one example of the application of the LQG/LTR design technique (i.e., linear quadratic gaussian (LQG) control with loop transfer recovery (LTR) procedure) to designing a robust controller for a series parallel resonant dc-dc converter can be found in [16].

Therefore, taking into consideration the above analysis of the state of the art of the applications of robust control techniques to designing controllers for power converters, it can be seen that most of the applications of the robust control theory have been aimed at improving the response of boost converters and $\acute{C}$uk converters.

Furthermore, they have been focused on the application of the LQR controller design technique, the LQG/LTR controller design technique, the standard $\mathcal{H}_\infty$ controller design technique, the nonlinear $\mathcal{H}_\infty$ controller design technique and the μ synthesis with DK iteration controller design technique.

However, there are other controller design techniques that are very powerful tools for the design of robust controllers. For example, the $\mathcal{H}_\infty$ loop-shaping controller design. In short, this technique is a two stage design process based on $\mathcal{H}_\infty$ robust stabilization combined with classical loop shaping [17, 18].

Moreover, important advantages of the $\mathcal{H}_\infty$ loop-shaping controller design technique are that no problem-dependent uncertainty and no γ-iteration for its solution are required.

In the present paper a robust controller for a buck-boost dc-dc power converter by using $\mathcal{H}_\infty$ loop-shaping control was designed [3–5,17, 18]. Moreover, in order to carry out a comparison between classical control and post-modern control, here the $\mathcal{H}_\infty$ loop-shaping controller is compared with a robust proportional-integral-derivative (PID) controller.

The results are satisfactory and show the importance of using robust controllers when designing the feedback-control loop of power converters.

2 The Buck-Boost Converter

In this paper, the state-space averaging procedure [19, 20] has been employed for the determination of the transfer function from the duty cycle to the output voltage. Fig. 1 shows the low-power buck-boost converter used in this paper; and Fig. 2 shows the circuits for developing the state equations, this figure includes the equivalent series resistance of the inductor and the capacitor. Here, the switching frequency is 250 kHz, the nominal input voltage is 12 V and the output voltage is -12 V.

It is assumed for simplicity that the converter is operated so that either the transistor or the diode is always conducting; this assumption rules out the discontinuous conduction mode, in which both devices are off during some part of each cycle.

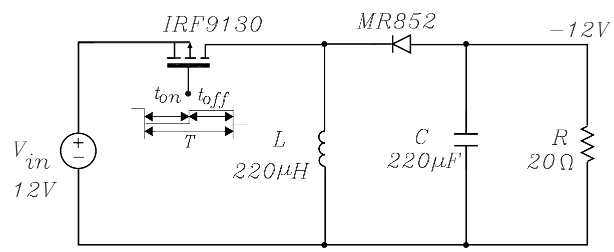

Figure 1: The buck-boost converter of this paper

Then, with the assumption of real components, (1) and (2) show the finite dimensional linear time invariant dynamical model of the system, where $x(t)$ is the system state vector, $d(t)$ is the system input (the duty cycle), and $v_o(t)$ is the system output (the voltage across the output capacitor).

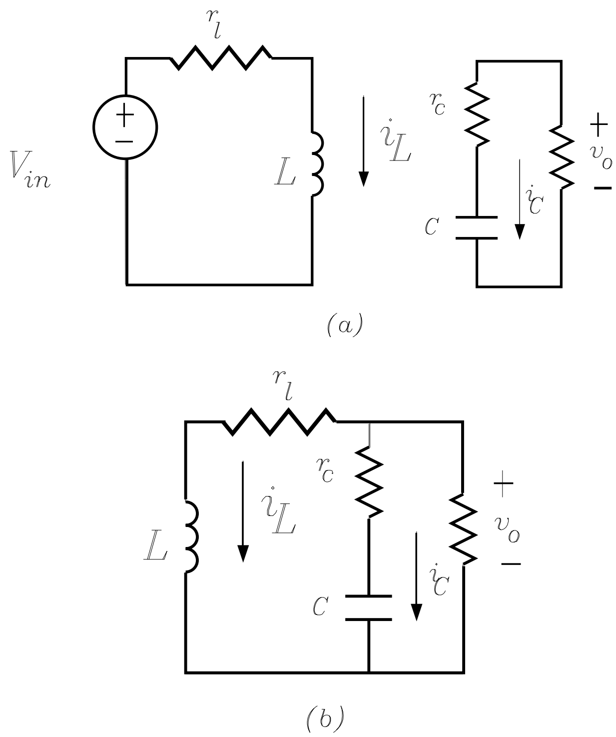

Figure 2: Circuits for developing the state equations for the buck-boost converter: (a) Switch closed; (b) Switch open.

In (3), the corresponding transfer function from $d(s)$ to $v_o(s)$ is defined, where $v_o(s)$ and $d(s)$ are the Laplace transforms of $v_o(t)$ and $d(t)$ with zero initial conditions ($x(0) = 0$).

$$\begin{aligned} \dot{x}(t) &= \overline{A}x(t) + \overline{B}d(t) && (1) \\ v_o(t) &= \overline{C}x(t) + \overline{D}d(t) && (2) \\ v_o(s) &= [\overline{C}(sI - \overline{A})^{-1}\overline{B} + \overline{D}]d(s) && (3) \end{aligned}$$

where

$$x(t) = \begin{bmatrix} i_L(t) \\ v_C(t) \end{bmatrix}$$

$$\overline{A} = \begin{bmatrix} -\frac{(R+r_C)r_L + Rr_C(1-D)}{(R+r_C)L} & \frac{R(1-D)}{(R+r_C)L} \\ -\frac{R(1-D)}{(R+r_C)C} & -\frac{1}{(R+r_C)C} \end{bmatrix}$$

$$\overline{B} = \begin{bmatrix} \frac{(R^2(1-D)+R(r_C+r_L)+r_C r_L)V_{in}}{L(r_L(R+r_C)+Rr_C(1-D)+R^2(1-D)^2)} \\ \frac{RDV_{in}}{(r_L(R+r_C)+Rr_C(1-D)+R^2(1-D)^2)C} \end{bmatrix}$$

$$\overline{C} = \begin{bmatrix} \frac{-Rr_C(1-D)}{R+r_C} & \frac{R}{R+r_C} \end{bmatrix}$$

$$\overline{D} = \frac{Rr_C DV_{in}}{r_L(R+r_C) + Rr_C(1-D) + R^2(1-D)^2}$$

Here, D represents the DC component of the duty cycle, $i_L(t)$ is the inductor current, $v_C(t)$ is the capacitor voltage, and I_L and V_C represent the DC components of the inductor current and the capacitor voltage, respectively. Also, r_L and r_C represent the effect of the equivalent series resistance of the inductor and the capacitor, respectively, and V_{in} is the DC component of the input voltage. Therefore, in accordance with [2], if it is assumed for a moment that $r_L = 0$, then (4) shows the transfer function from the duty cycle to the output voltage.

$$\frac{v_o(s)}{d(s)} = \frac{V_{in}}{LC} \cdot \frac{(s\frac{LD}{R(1-D)^2} - 1)(sCr_C + 1)}{s^2 + s\frac{L+Rr_C C(1-D)}{LCR} + \frac{(1-D)^2}{LC}} \quad (4)$$

For the purpose of this paper, the equivalent series resistance of the power transistor and the diode have been neglected. However, according to [2], r_L and r_C have not been neglected. Therefore, if we take into account that for this paper $r_L = 0.2\ \Omega$, $r_C = 0.1\ \Omega$ and $D = 0.53$, then for the values shown in Fig. 1, the transfer function from the duty cycle to the output voltage is given by (5).

$$G_p(s) = \frac{v_o(s)}{d(s)} = 0.1363 \cdot \frac{N_p(s)}{D_p(s)} \quad (5)$$

where

$$\begin{aligned} N_p(s) &= (s + 45455)(s - 38696) \\ D_p(s) &= s^2 + 1347.81s + 4.77 \cdot 10^6 \end{aligned}$$

3 Robust Controller Design

In the previous section, the transfer function from the duty cycle to the output voltage was given. However, it is important to say that no single fixed model can respond exactly like the true plant. According to Zhou et al. [4], the universe of mathematical models from which a model set is chosen is distinct from the universe of physical systems. For this reason, a model set which includes the true physical plant can never be constructed. In a nutshell, the designer is faced with both *structured uncertainties* and *unstructured uncertainties*. The first ones are due to the fact that the exact value of the parameters of the structure of the model is unknown and such parameters also vary with aging, perturbations, and so on. In addition, the second uncertainties are due to the fact that, for high frequency signals, the parameterized finite dimensional linear time invariant model fails to describe the plant because the plant will always have dynamics which are not represented in the fixed order model.

The above-mentioned uncertainties negatively affect parameters that define the dynamics of the process such as the inductor current and the capacitor voltage.

With this scenario in mind, designing a robust controller for power converters is not an easy task. However, for a single-input-single-output (SISO) plant, if the designer guarantees that the system has a gain margin equal to infinity, a gain reduction margin equal to 0.5 and a (minimum) phase margin of 60^o, the robustness of the controlled system is guaranteed [4, 5].

This paper's buck-boost dc-dc power converter is based on pulse-width-modulation (PWM) techniques and the voltage-mode PWM mode of operation was used. Moreover, in order to know whether the feedback-controlled system contains hidden unstable modes, an internal stability analysis of the closed-loop system was made.

3.1 Internal Stability

In this paper, in order to carry out the internal stability analysis of the feedback-controlled system, the block diagram shown in Fig. 3 was used. It consists of the plant $G_p(s)$, the controller $C(s)$, the plant output disturbance ω_1, the plant input disturbance ω_2, the controller input signal z_1 and the plant input signal z_2.

Assume that the feedback-controlled system is well-posed and that neither $G_p(s)$ nor $C(s)$ have hidden unstable modes [4]. The system shown in Fig. 3 can be given by

$$\begin{bmatrix} z_1 \\ z_2 \end{bmatrix} = T(s) \begin{bmatrix} \omega_1 \\ \omega_2 \end{bmatrix} \tag{6}$$

where

$$T(s) = \begin{bmatrix} T_{11}(s) & T_{12}(s) \\ T_{21}(s) & T_{22}(s) \end{bmatrix} \tag{7}$$

and

$$\begin{aligned} T_{11}(s) &= (I + G_pC)^{-1} \\ T_{12}(s) &= G_p(I + CG_p)^{-1} \\ T_{21}(s) &= -C(I + G_pC)^{-1} \\ T_{22}(s) &= (I + CG_p)^{-1} \end{aligned}$$

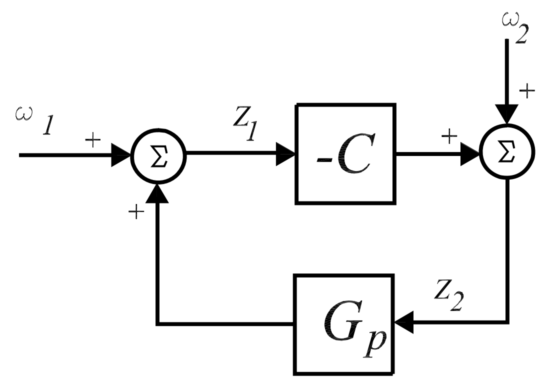

Figure 3: Diagram used to carry out the internal stability analysis.

Theorem 1 *The feedback-controlled system in Fig. 3 is internally stable if the internal signals (i.e., z_1 and z_2) are bounded for all bounded inputs (i.e., ω_1 and ω_2).*

Proof: An excellent proof of this theorem can be found in Chapter 5 of Zhou et al. [4].

According to Skogestad and Postlethwaite [5], the feedback-controlled system shown in Fig. 3 is internally stable if $T(s)$ in (7) is stable.

According to Youla et al. [21], all the stabilizing controllers for this paper's power converter can be parameterized. *Lemma 1* is due to the Youla-parameterization or Q-parameterization.

Lemma 1 *For the case under analysis, $G_p(s)$ is a stable plant, the closed-loop system in Fig. 3 is internally stable provided that*

$$Q = C\,(I + G_pC)^{-1}$$

is stable.

Proof: An excellent proof of this lemma can be found in Skogestad and Postlethwaite [5].

3.2 PID Controller Design

Among all the classical control techniques developed over the years, PID control stands out as one of the most effective control technique when meeting the performance specifications of feedback-controlled systems. The PID-controller is the most widely used controller in the process industry and its transfer function is given by

$$C(s) = \Pi_p + \Pi_d s + \frac{\Pi_i}{s} \qquad (8)$$

which can be written as

$$C(s) = \left(\frac{\Pi_d s^2 + \Pi_p s + \Pi_i}{s} \right)$$

where the gains Π_p, Π_d and Π_i are the PID coefficients [22].

In (8), it can be seen that $C(s)$ involves differentiation of the input, it is an improper transfer function.

Experience tells us that (8) can be transformed into a proper transfer function by letting the derivative action be effective only over a limited frequency range [5].

Thus, in order to limit the derivative action, the transfer function given by (8) can be changed into the following transfer function

$$C(s) = \Pi_p + \frac{\Pi_d s}{(\epsilon \Theta_d s + 1)} + \frac{\Pi_i}{s} \qquad (9)$$

where $\epsilon \leq 0.1$ and Θ_d is the derivative time constant. Therefore, (9) can be re-written as

$$C(s) = \frac{\Pi_d + \epsilon \Theta_d \Pi_p}{\epsilon \Theta_d} \cdot \frac{N_1(s)}{D_1(s)} \qquad (10)$$

where

$$\begin{aligned} N_1(s) &= s^2 + \frac{\Pi_p + \epsilon \Theta_d \Pi_i}{\Pi_d + \epsilon \Theta_d \Pi_p} s + \frac{\Pi_i}{\Pi_d + \epsilon \Theta_d \Pi_p} \\ D_1(s) &= s \left(s + \frac{1}{\epsilon \Theta_d} \right) \end{aligned}$$

For the problem at hand, a PID-controller that gave a closed-loop system with robust stability margins (i.e., phase margin = 60.4^o and gain margin = 17.31 dB) was

$$C(s) = -\frac{(s + 1934.8)^2}{s\,(s + 45455)} \qquad (11)$$

The loop transfer function is given by

$$L(s) = G_p(s) C(s)$$

where $G_p(s)$ is given by (5) and $C(s)$ is given by (11).

Finally, for this paper's PID-controller, it can also be checked that $T(s)$ (see (7)) is stable. Therefore, the closed-loop system is internally stable.

3.3 $\mathcal{H}_\infty$ Loop-Shaping Controller Design

In the present paper, the one degree-of-freedom (1DOF) $\mathcal{H}_\infty$ loop-shaping design procedure was also used [18]. Excellent information on $\mathcal{H}_\infty$ loop-shaping control can also be found in [3–5].

In this control technique, the converter's transfer function $G_p(s)$ (see (5)) is represented as the following left coprime factor perturbed plant

$$G_p{}^U = (O + U_O)^{-1} (R + U_R) \qquad (12)$$

where the transfer functions U_O and U_R are stable and unknown. They represent the uncertainty in $G_P(s)$. In addition,

$$\left\| \left[\begin{array}{cc} U_R & U_O \end{array} \right] \right\|_\infty < \delta \qquad (13)$$

where δ is the stability margin $(0 < \delta)$ [3–5]. Fig. 4 shows the block diagram of the 1DOF $\mathcal{H}_\infty$ loop-shaping design problem.

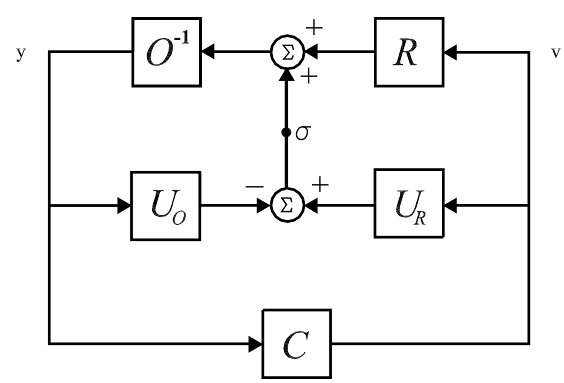

Figure 4: Block diagram of the 1DOF $\mathcal{H}_\infty$ loop-shaping design problem.

According to Skogestad and Postlethwaite [5], the feedback-controlled system shown in

Fig. 4 is robustly stable provided that

$$\gamma \triangleq \left\| \begin{bmatrix} C \\ I \end{bmatrix} (I - G_p C)^{-1} O^{-1} \right\|_\infty$$

be

$$\gamma \leq \frac{1}{\delta} \quad (14)$$

where the symbol $\triangleq$ denotes *equal by definition*. Here, the $\mathcal{H}_\infty$ control problem is to find a robust and optimal controller that guarantees that (14) holds.

Finally, according to Glover and McFarlane [17] and Skogestad and Postlethwaite [5], the minimum value of γ_{min} and the maximum stability margin δ_{max} are given by

$$\gamma_{min} = \frac{1}{\delta_{max}} = \left(1 - \left|\left|\left[\begin{array}{cc} R & O \end{array}\right]\right|\right|_H^{-\frac{1}{2}}\right)^{-\frac{1}{2}} \quad (15)$$

where $||\cdot||_H$ denotes Hankel norm. An efficient procedure to find a controller that robustly stabilizes a given shaped plant with respect to coprime factor uncertainty using $\mathcal{H}_\infty$ optimization is given by Skogestad and Postlethwaite [5] (Chapter 9, p. 378). In addition, the MATLAB function *coprimeunc* can be used to obtain the above-mentioned controller.

In order to carry out the controller design process, the plant $G_p(s)$ (5) was shaped by using the pre-compensator $F(s)$ given by

$$F(s) = -0.02 \frac{s + 1.3 \cdot 10^3}{s} \quad (16)$$

Therefore, the shaped plant was given by

$$G_p{}^S(s) = G_p(s) F(s) \quad (17)$$

and, using the MATLAB function *coprimeunc*, the $\mathcal{H}_\infty$ loop-shaping positive-feedback controller given by (18) was obtained.

$$C(s) = 2.7 \cdot 10^{-3} \cdot \frac{N_2(s)}{D_2(s)} \quad (18)$$

where

$$N_2(s) = s^3 - 4.6 \cdot 10^6 s^2 - 5.7 \cdot 10^9 s - 1.3 \cdot 10^{13}$$
$$D_2(s) = s^3 + 1.3 \cdot 10^4 s^2 + 5.7 \cdot 10^7 s + 5.8 \cdot 10^{10}$$

In order to guarantee tracking, the gain K_0 given by

$$K_0 = C(0) = -0.6253$$

was placed between at the system input.

In this case, the loop transfer function is given by

$$L(s) = G_p{}^S(s) C(s)$$

where $G_p{}^S(s)$ is the shaped plant given by (17) and $C(s)$ is the controller given by (18).

For this paper's $\mathcal{H}_\infty$ loop-shaping controller (18), the system also had robust stability margins (i.e., phase margin = 88.4^o and gain margin = 17.63 dB). Furthermore, γ_{min} was equal to 1.73, which is a satisfactory value of γ_{min} [5].

Moreover, for the controller given by (18), it can also be checked that the feedback-controlled system is internally stable.

4 Experimental Results

The prototype of the buck-boost converter tested in the laboratory is shown in Fig. 5.

Figure 5: Prototype of the buck-boost converter tested in the laboratory.

Also, Fig. 6 shows a schematic representation of the implementation of the PID-controller (11), where $R_1 = 98.43\ \Omega$, $C_1 = 5.25\ \mu$F, $R_2 = 5.17$ kΩ, $C_2 = 100$ nF and $C_3 = 4.45$ nF. In that figure, the resistors and capacitors with nonstandard values were implemented by using classical techniques of linear circuit analysis for the connection passive components.

Furthermore, a block diagram of the closed-loop system by using the PID-controller is shown in Fig. 7. Here, the PWM actuator was implemented by using the National Semiconductor Regulating Pulse Width Modulator LM3524D.

Experimental results of the response of the PID-controlled buck-boost converter to a rectangular perturbation in the input voltage of $\pm$ 2.4 V at 50 Hz are shown in Fig. 8.

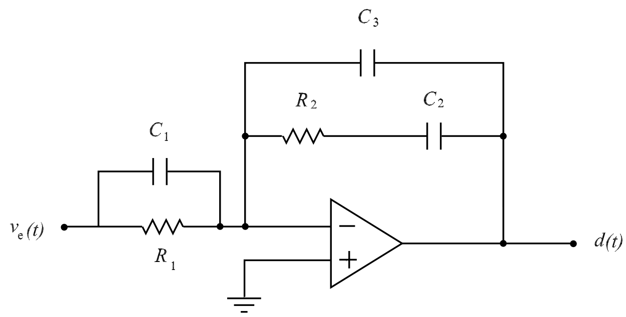

Figure 6: Schematic representation of the PID control for the buck-boost converter.

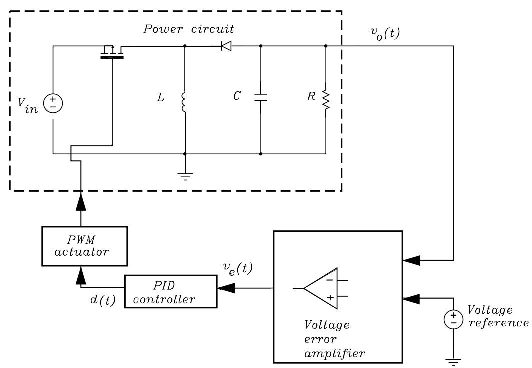

Figure 7: Block diagram of the closed-loop system by using the PID-controller.

Also, experimental results of the response of the PID-controlled buck-boost converter to a rectangular perturbation in the load of ± 220 mA at 50 Hz are shown in Fig. 9. Here, the PWM actuator was implemented by using the National Semiconductor Regulating Pulse Width Modulator LM3524D.

At the beginning of this research, the robust controller given by (18) was implemented by using analog electronics (operational amplifiers and passive electrical components). However, such a practical implementation had some drawbacks. For instance, the practical implementation of the transfer function given by (18) was much more complex than the one of the PID-controller given by (11). In addition, the characteristics of that analog controller could not be changed easily when such changes were needed. For these reasons, among others, in this research it was decided to discard the practical implementation of (18) as an analog controller.

Therefore, here the implementation of (18) was carried out by using computer assistance as a digital controller, as in [12].

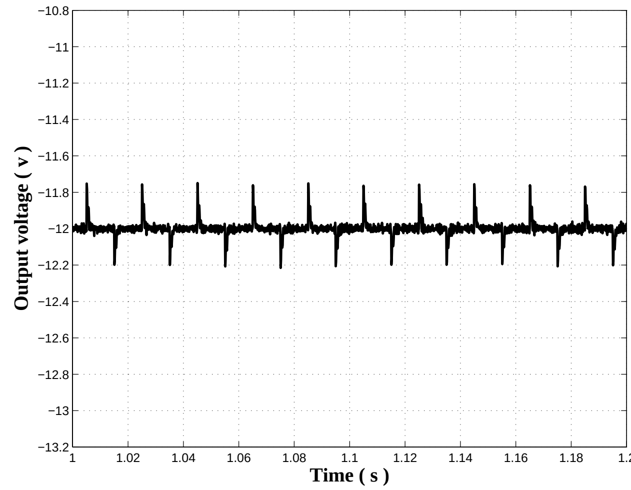

Figure 8: Experimental results of the response of the PID-controlled buck-boost converter to a rectangular perturbation in the input voltage of ± 2.4 V at 50 Hz.

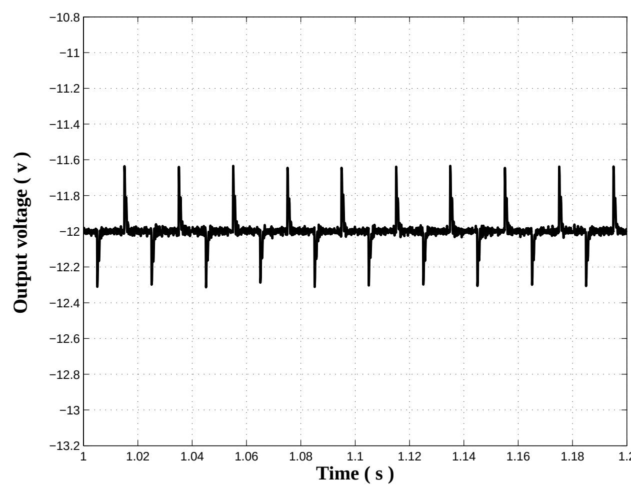

Figure 9: Experimental results of the response of the PID-controlled buck-boost converter to a rectangular perturbation in the load of ± 220 mA at 50 Hz.

Data processing in the digital controller was straightforward, complex calculations could be performed easily, controller characteristics could be changed easily when such changes were needed, and the digital controller was far superior to the corresponding analog controller from the point of view of internal noise and drift effects.

Fig. 10 shows the block diagram of the digital control system. In addition, for a sampling rate of 4 kHz and applying the *bilinear transformation*, the pulse transfer function of the 1DOF $\mathcal{H}_\infty$ loop-shaping controller given by (18) multiplied by the pre-compensator given by (16) is the one given by

$$C(z) = \frac{N_3(z)}{D_3(z)} \tag{19}$$

where

$$N_3(z) = b_o + b_1 z^{-1} + b_2 z^{-2} + b_3 z^{-3} + b_4 z^{-4}$$
$$D_3(z) = 1 + a_1 z^{-1} + a_2 z^{-2} + a_3 z^{-3} + a_4 z^{-4}$$

and

$$\begin{aligned} a_1 &= -1.9321 \\ a_2 &= 1.1640 \\ a_3 &= -0.2790 \\ a_4 &= 0.0471 \\ b_o &= 0.0120 \\ b_1 &= -0.0156 \\ b_2 &= -0.0052 \\ b_3 &= 0.0162 \\ b_4 &= -0.0064 \end{aligned}$$

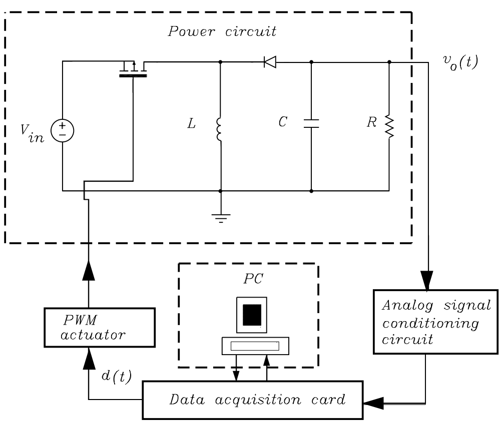

Figure 10: Block diagram of the digital control system. 1DOF $\mathcal{H}_\infty$ loop-shaping control.

Here, (19) was implemented by using the National Instruments Data Acquisition Card NI DAQCard-6062E.

Experimental results of the response of the 1DOF $\mathcal{H}_\infty$ loop-shaping-controlled buck-boost converter to a rectangular perturbation in the input voltage of ± 2.4 V at 50 Hz are shown in Fig. 11, and experimental results of the response of the 1DOF H_∞ loop-shaping-controlled buck-boost converter to a rectangular perturbation in the load of ± 220 mA at 50 Hz are shown in Fig. 12.

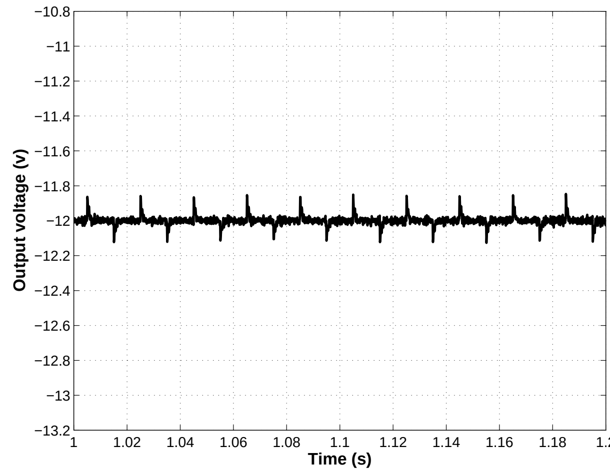

Figure 11: Experimental results of the response of the 1DOF H_∞ loop-shaping-controlled buck-boost converter to a rectangular perturbation in the input voltage of ± 2.4 V at 50 Hz.

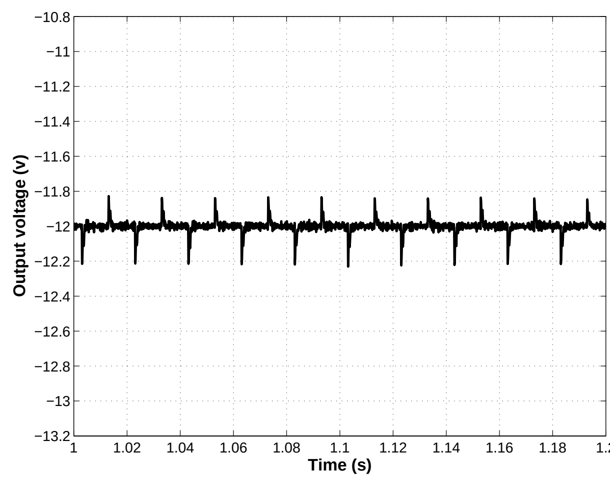

Figure 12: Experimental results of the response of the 1DOF $\mathcal{H}_\infty$ loop-shaping-controlled buck-boost converter to a rectangular perturbation in the load of ± 220 mA at 50 Hz.

The above experimental results show that the buck-boost converter implemented by using the post-modern controller attenuates input ripple at 50 Hz better than the buck-boost converter implemented by using the classical controller (see Fig. 8 and Fig. 11).

Second, in spite of the fact that Fig. 9 and Fig. 12 indicate a satisfactory rejection of both controlled systems to load current ripple at 50 Hz, the aforementioned two figures also show that the $\mathcal{H}_\infty$ loop-shaping-controlled buck-boost converter is superior to the PID-controlled buck-boost converter.

On the other hand, the practical implementation of the PID-controller (11) was much more easier than the one of the $\mathcal{H}_\infty$ loop-shaping controller (18). The latter required computer assistance.

To sum up, it should be highlighted that in spite of the fact that the performance of the $\mathcal{H}_\infty$-controlled buck-boost dc-dc power converter was better than the performance of the PID-controlled power converter, it can be said that the performances of both robust designs were satisfactory.

Other applications of general robust control techniques to improve the performance of electrical systems that have yielded satisfactory results can be found in [23–25]

5 Conclusion

To conclude, in this paper two robust controllers have been designed in order to build a robust buck-boost dc-dc power converter. One of the controllers was designed by using classical control techniques and the other was designed by using post-modern ones.

The results of the experiments were satisfactory and showed that both controllers allowed the buck-boost converter to reject perturbations in the input voltage and in the load current satisfactorily.

Also, these results showed that none of the robust controllers presented in this paper depend strongly on the operating point. Both controllers satisfactorily met the desired closed-loop system behavior.

Comparing both robust controllers, the results of the experiment also showed that the 1DOF $\mathcal{H}_\infty$ loop-shaping controller performed better than the PID-controller.

The $\mathcal{H}_\infty$-controlled converter attenuates both input ripple and perturbations in the load current at 50 Hz better than the buck-boost converter implemented by using the PID-controller.

Acknowledgements: This research has been partially supported by the Universidad Politecnica de Madrid under the research projects Q065904150 and M0800204113, and by the Ministry of Education and Science (MEC) of Spain under the research project TEC2007-63121.

References:

[1] S. Hiti and D. Borojević, Robust nonlinear control for boost converter, *IEEE Transactions on Power Electronics*, Vol. 10, 1995, No. 6, pp. 651–658.

[2] R. Naim, G. Weiss, and S. Ben-Yaakov, $\mathcal{H}_\infty$ control applied to boost power converters, *IEEE Transactions on Power Electronics*, Vol. 12, No. 4, 1997, pp. 677–683.

[3] M. Green and D. J. N. Limebeer, *Linear Robust Control,* Prentice–Hall, 1996.

[4] K. Zhou, J. C. Doyle, and K. Glover, *Robust and Optimal Control,* Prentice–Hall, 1996.

[5] S. Skogestad and I. Postlethwaite, *Multivariable Feedback Control,* John Wiley & Sons, 1996.

[6] B. Francis, *A Course in $\mathcal{H}_\infty$ Control Theory,* Springer-Verlag, 1987.

[7] T. Chen and B. Francis, *Optimal Sampled-Data Control Systems,* Springer-Verlag, 1995.

[8] S. P. Bhattacharyya, H. Chapellat and L. H. Keel, *Robust Control: The Parametric Approach,* Prentice–Hall, 1995.

[9] J. B. Burl, *Linear Optimal Control: $\mathcal{H}_2$ and $\mathcal{H}_\infty$ Methods,* Addison-Wesley, 1999.

[10] S. Buso, Design of a robust voltage controller for a buck-boost converter using μ-synthesis, *IEEE Transactions on Control Systems Technology*, Vol. 7, No. 2, 1999, pp. 222–229.

[11] A. Van der Schaft, *L_2-Gain and Passivity Techniques in Nonlinear Control,* 2nd ed., Springer–Verlag, 2000.

[12] A. Kugi and K. Schlacher, Nonlinear $\mathcal{H}_\infty$-controller design for a dc-to-dc power converter, *IEEE Transactions on Control Systems Technology,* Vol. 7, No. 2, 1999, pp. 230–237.

[13] G. F. Wallis and R. Tymerski, A generalized approach for μ synthesis of robust switching regulators, *IEEE Transactions on Aerospace and Electronic Systems,* Vol. 36, No. 2, 2000, pp. 422-431.

[14] H. Vidal–Idiarte, L. Martínez–Salamero, H. Valderrama–Blavi, F. Guinjoan, and J. Maxé, Analysis and design of a $\mathcal{H}_\infty$ control of nonminimu phase-switching converters, *IEEE Transactions on Circuits and Systems-I: Fundamental Theory and Applications,* Vol. 50, No. 10, 2003, pp. 1316-1323.

[15] F. H. F. Leung, P. K. S. Tam, and C. K. Li, An improved LQR-based controller for switching dc-dc converters, *IEEE Transactions on Industrial Electronics,* Vol. 40, No. 5, 1993, pp. 521-528.

[16] O. Ojo, Robust control of series parallel resonant converters, *IEE Proceedings - Control Theory and Applications,* Vol. 142, 1995, pp. 401-410.

[17] K. Glover and D. McFarlane, Robust stabilization of normalized coprime factor plant descriptions with $\mathcal{H}_\infty$ bounded uncertainty, *IEEE Transactions on Automatic Control,* Vol. 34, No. 8, 1989, pp. 821-830.

[18] D. McFarlane and K. Glover, *Robust Controller Design Using Normalized Coprime Factor Plant Descriptions,* Springer-Verlag, 1990.

[19] R. D. Middlebrook and S. Ćuk, A general unified approach to modelling switching-converter power stages, *IEEE Power Electronics Specialist Conference,* 1976, pp. 18–34.

[20] K. K. Sum, *Switch Mode Power Conversion: Basic theory and design,* Marcell Dekker, 1984.

[21] D. C. Youla, H. A. Jabr, and J. J. Bongiorno, Modern Wierne-Hopf design of optimal controllers, part II: The multivariable case, *IEEE Transactions on Automatic Control,* Vol. 21, No. 3, 1976, pp. 319–338.

[22] K. Ogata, *Modern Control Engineering,* 3rd ed., Prentice-Hall, 1997.

[23] M. Rafiei, R. Ghazi, R. Asgharian, H. A. Toliyat, and M. Barakati, Robust control methodologies for dc/dc PWM converters under wide changes in operating conditions, *WSEAS Transactions on Systems,* Issue 11, Vol. 5, 2006, pp. 255-265.

[24] P. Cadotte, H. Michalska, and B. Boulet, Robust Stability Analysis of an Electronic Circuit System with $\mathcal{L}_\infty$ - Performance Objectives and Repeated Perturbations, *WSEAS Transactions on Systems,* Issue 6, Vol. 4, 2005, pp. 726-735.

[25] L. Garcia, M. J. Lopez, and J. Lorenzo, Robust LQG/LTR Controller and Fault Detection Method for Aircraft Sensors and Actuators Based on Genetic Algorithms, *WSEAS Transactions on Systems,* Issue 11, Vol. 4, 2005, pp. 2016-2022.